



Research paper

Syntheses, crystal structures, and solid-state spectroscopic properties of helical and non-helical dinuclear zinc(II) complexes derived from N₂O₂ ligands with different torsion-generating sources

Yuuki Oshikawa, Ko Yoneda, Masayuki Koikawa, Yasunori Yamada*

Department of Chemistry and Applied Chemistry, Faculty of Science and Engineering, Saga University, 1 Honjo-machi, Saga 840-8502, Japan

ARTICLE INFO

Keywords:

Dinuclear zinc(II) complexes
N₂O₂ ligands
Crystal structures
Helicates
Photoluminescence

ABSTRACT

The reaction of bis(*N*-salicylidene)-4,4'-diaminodiphenyl)ether (⁴OsalH₂) with zinc(II) ion affords a 2:2 dinuclear zinc(II) complex formulated as [Zn₂(⁴Osal)₂]. A similar 2:2 dinuclear zinc(II) complex, [Zn₂(⁴Ssal)₂], can be obtained by the reaction of bis(*N*-salicylidene)-4,4'-diaminodiphenyl)thioether (⁴SsalH₂) with zinc(II) ion. These two complexes, [Zn₂(⁴Osal)₂] and [Zn₂(⁴Ssal)₂], take similar helical structures. Although bis(*N*-salicylidene)-3,3'-diaminodiphenyl)methane (³MsalH₂) and bis(*N*-salicylidene)-2,2'-diaminodiphenyl)thioether (²SsalH₂) give dinuclear complexes with similar compositions, [Zn₂(³Msal)₂] and [Zn₂(²Ssal)₂], respectively, their structures are quite different from those of [Zn₂(⁴Osal)₂] and [Zn₂(⁴Ssal)₂]. Namely, [Zn₂(³CH₂sal)₂] and [Zn₂(²Ssal)₂] take the mosocate and the phenoxo-bridged dinuclear structures, respectively. Such structural differences between the formed complexes occur depending on the relative positions of the two amino groups of the precursor dianiline, and reflect their diffuse reflectance and photoluminescence spectral behaviours. It has become clear that the electronic transitions of such a complex strongly depend on the relative arrangement of the two amino groups in the precursor dianiline compound as well as the kind of the central atom linking two aniline frameworks.

1. Introduction

Metal complexes with helical structures have been attracting much attention for their characteristic stereochemistry and possible multifunctionality [1–18]. For constructing such helical complexes, coordination modes of incorporated metal ions and/or stereochemistry of used multidentate ligands can be regarded as key factors [2,4]. As for the latter multidentate ligands, in particular, a variety of approaches have been taken so far [4]. In most cases, however, complicated synthetic procedures are adopted, and hence the development of the related study is disturbed. From such viewpoints, bis(4-aminophenyl)methane or its analogue is prominent precursor for the ligand that induces helical structure [19–34]. In the case of bis(4-aminophenyl)methane, for instance, a simple condensation with salicylaldehyde results in the formation of bis(*N*-salicylidene)-4,4'-diaminodiphenyl)methane (⁴CH₂salH₂), in which the central methylene group can act as a torsion-generating source [24]. Actually, the reaction of ⁴CH₂salH₂ with Zn²⁺ ion affords a double helical complex, [Zn₂(⁴CH₂sal)₂] [24]. In this type ligand, furthermore, the central torsion-generating group can be replaced to ether (⁴OsalH₂) and thioether (⁴SsalH₂) by using the

corresponding precursors, bis(4-aminophenyl)ether and bis(4-aminophenyl)thioether, respectively. Although these ligands are expected to possess similar coordination abilities to ⁴CH₂salH₂, stereochemistry and/or spectroscopic properties depending on the torsion-generating groups of their complexes remain equivocal. For similar ligands with N₂O₂ donor sets, on the other hand, it has been found that the positional relations between two amino groups in precursors significantly affect the structures of the resulting complexes [35–40]. By analogy with this fact, the probability of formation of the helical structure may depend on the positional factor of the two amino groups in the precursor for the present ligand system. In the case of the ligand with N₄ donor sets derived from the same precursor, actually, not only a helical complex but also a non-helical box-type complex can be obtained depending on the positions of the amino groups [19,20,22,41]. However, there are many unclear points about the correlation between the positions of the amino groups and the resulting polynuclear structures. In the present work, we will describe syntheses, structures, and spectroscopic properties of dinuclear zinc(II) helical complexes derived from three types of N₂O₂ ligands, ⁴CH₂salH₂, ⁴OsalH₂, and ⁴SsalH₂, with different torsion-generating sources. The structures and spectroscopic

* Corresponding author.

E-mail address: yyamada@cc.saga-u.ac.jp (Y. Yamada).<https://doi.org/10.1016/j.ica.2019.118979>

Received 26 April 2019; Received in revised form 24 June 2019; Accepted 24 June 2019

Available online 28 June 2019

0020-1693/ © 2019 Elsevier B.V. All rights reserved.

properties of another-type zinc(II) complexes with similar N_2O_2 ligands, 3CH_2salH_2 and 2SsalH_2 , whose precursors are bis(3-aminophenyl)methane and bis(2-aminophenyl)thioether, respectively, were also compared and examined.

2. Experimental

2.1. Materials and measurements

$Zn(CH_3COO)_2 \cdot 2H_2O$, salicylaldehyde, bis(4-aminophenyl)methane, bis(3-aminophenyl)methane, bis(4-aminophenyl)ether, bis(4-aminophenyl)thioether, bis(2-aminophenyl)thioether, NaOH, triethylamine, and other chemicals were commercially available and used as received. The ligand, 4CH_2salH_2 , and the dinuclear zinc(II) complex, $[Zn_2({}^4CH_2sal)_2]$, were synthesized following literature procedures [24]. Elemental analyses (C, H, N) were performed with a Perkin-Elmer 2400 CHN Elemental Analyzer. Diffuse reflectance spectra were measured with a Perkin-Elmer Lambda 900Z spectrophotometer equipped with an integrating sphere apparatus. IR spectra were recorded on a Bruker VERTEX 70 FT/IR spectrometer. Photoluminescence and excitation spectra were recorded with a Jasco FP-6200 spectrophotometer. Photoluminescence quantum yields were measured by using a HAMAMATSU Quantaurus-QY absolute PL quantum yield spectrometer. Emission lifetime measurements were conducted by using an EDINBURGH INSTRUMENTS OB920 fluorescence lifetime spectrometer. The lifetime of each compound was estimated from the fluorescence decay curves by software followed with one exponential decay kinetics.

2.2. Synthesis of 4OsallH_2

The ligand, 4OsallH_2 , was prepared by a similar method to that for 4CH_2salH_2 , using bis(4-aminophenyl)ether instead of bis(4-aminophenyl)methane [24]. To a solution containing salicylaldehyde (0.61 g, 5.0 mmol) in ethanol (30 cm^3) was added bis(4-aminophenyl)ether (0.50 g, 2.5 mmol). After the mixture was stirred at 78 °C for 3 h, the resultant yellow powder was collected by filtration. Yield = 0.98 g (96%). *Anal. Calc.* for $C_{26}H_{20}N_2O_3$ (4OsallH_2): C, 76.45; H, 4.94; N, 6.86%. Found: C, 76.50; H, 4.97; N, 6.80%. Characteristic IR data [cm^{-1}]: 1280^s, 1608^s, 2700^{br}. Diffuse reflectance spectrum [λ_{max} , nm] (relative intensity respect to the 418.0 nm band): 418.0 (1.00), 319.5 (0.91), 238.0 (0.48).

2.3. Synthesis of 4SsalH_2

The ligand, 4SsalH_2 , was prepared by a similar method to that for 4OsallH_2 , using bis(4-aminophenyl)thioether instead of bis(4-aminophenyl)ether. To a solution containing salicylaldehyde (0.61 g, 5.0 mmol) in ethanol (30 cm^3) was added bis(4-aminophenyl)thioether (0.54 g, 2.5 mmol). After the mixture was stirred at 78 °C for 3 h, the resultant yellow powder was collected by filtration. Yield = 0.98 g (86%). *Anal. Calc.* for $C_{26}H_{20}N_2O_2S$ (4SsalH_2): C, 73.56; H, 4.75; N, 6.60%. Found: C, 73.57; H, 4.80; N, 6.55%. Characteristic IR data [cm^{-1}]: 1280^s, 1608^s, 2700^{br}. Diffuse reflectance spectrum [λ_{max} , nm] (relative intensity respect to the 418.0 nm band): 418.0 (1.00), 319.5 (0.91), 238.0 (0.48).

2.4. Synthesis of 3CH_2salH_2

The ligand, 3CH_2salH_2 , was prepared by a similar method to that for 4CH_2salH_2 , using bis(3-aminophenyl)methane instead of bis(4-aminophenyl)methane [24]. To a solution containing salicylaldehyde (0.61 g, 5.0 mmol) in ethanol (30 cm^3) was added bis(3-aminophenyl)methane (0.50 g, 2.5 mmol). After the mixture was stirred at 78 °C for 3 h, the resultant yellow powder was collected by filtration. Yield = 0.99 g (97%). *Anal. Calc.* for $C_{27}H_{22}N_2O_2$ (3CH_2salH_2): C, 79.78; H, 5.45; N, 6.89%. Found: C, 79.79; H, 5.49; N, 6.86%. Characteristic IR data

[cm^{-1}]: 1280^s, 1618^s, 2700^{br}. Diffuse reflectance spectrum [λ_{max} , nm] (relative intensity respect to the 418.0 nm band): 418.0 (1.00), 319.5 (0.91), 238.0 (0.48).

2.5. Synthesis of 2SsalH_2

The ligand, 2SsalH_2 , was prepared by a similar method to that for 4SsalH_2 , using bis(2-aminophenyl)thioether instead of bis(4-aminophenyl)thioether. To a solution containing salicylaldehyde (0.61 g, 5.0 mmol) in ethanol (30 cm^3) was added bis(2-aminophenyl)thioether (0.54 g, 2.5 mmol). After the mixture was stirred at 78 °C for 3 h, the resultant yellow powder was collected by filtration. Yield = 0.93 g (88%). *Anal. Calc.* for $C_{26}H_{20}N_2O_2S$ (2SsalH_2): C, 73.56; H, 4.75; N, 6.60%. Found: C, 73.60; H, 4.76; N, 6.54%. Characteristic IR data [cm^{-1}]: 1277^s, 1610^s, 2700^{br}. Diffuse reflectance spectrum [λ_{max} , nm] (relative intensity respect to the 418.0 nm band): 418.0 (1.00), 319.5 (0.91), 238.0 (0.48).

2.6. Synthesis of $[Zn_2({}^4Osall)_2]$

To a suspension containing 4OsallH_2 (0.082 g, 0.20 mmol) and NaOH (0.032 g, 0.80 mmol) in methanol (20 cm^3) was added $Zn(CH_3COO)_2 \cdot 2H_2O$ (0.044 g, 0.20 mmol). After the whole was stirred at ambient temperature for 5 h, the resultant fluorescent yellow powder was collected by filtration. X-ray quality crystals of the complex were obtained by recrystallization from a 1:1 mixed solvent of acetonitrile and dichloromethane. Yield = 0.081 g (86% based on Zn). *Anal. Calc.* for $C_{52}H_{36}N_4O_6Zn_2$ ($[Zn_2({}^4Osall)_2]$): C, 66.17; H, 3.84; N, 5.94%. Found: C, 66.20; H, 3.89; N, 5.88%. Characteristic IR data [cm^{-1}]: 1256^m (medium), 1604^s (strong). Diffuse reflectance spectrum [λ_{max} , nm] (relative intensity respect to the 419.0 nm band): 419.0 (1.00), 316 (0.9)^{sh} (shoulder), 239.0 (0.47).

2.7. Synthesis of $[Zn_2({}^4Ssal)_2]$

The complex, $[Zn_2({}^4Ssal)_2]$, was prepared by a similar method to that for $[Zn_2({}^4Osall)_2]$, using 4SsalH_2 instead of 4OsallH_2 . To a suspension containing 4SsalH_2 (0.085 g, 0.20 mmol) and NaOH (0.032 g, 0.80 mmol) in methanol (20 cm^3) was added $Zn(CH_3COO)_2 \cdot 2H_2O$ (0.044 g, 0.20 mmol). After the whole was stirred at ambient temperature for 5 h, the resultant fluorescent yellow powder was collected by filtration. X-ray quality crystals of the complex were obtained by recrystallization from a 1:1 mixed solvent of methanol and dichloromethane. Yield = 0.086 g (88% based on Zn). *Anal. Calc.* for $C_{52}H_{36}N_4O_4S_2Zn_2$ ($[Zn_2({}^4Ssal)_2]$): C, 64.01; H, 3.72; N, 5.74%. Found: C, 64.07; H, 3.75; N, 5.70%. Characteristic IR data [cm^{-1}]: 1252^m, 1601^s. Diffuse reflectance spectrum [λ_{max} , nm] (relative intensity respect to the 422.5 nm band): 422.5 (1.00), 313 (0.9)^{sh}, 238.5 (0.55).

2.8. Synthesis of $[Zn_2({}^3CH_2sal)_2]$

The complex, $[Zn_2({}^3CH_2sal)_2]$, was prepared by a similar method to that for $[Zn_2({}^4Osall)_2]$, using 3CH_2salH_2 instead of 4OsallH_2 . To a suspension containing 3CH_2salH_2 (0.081 g, 0.20 mmol) and NaOH (0.032 g, 0.80 mmol) in methanol (20 cm^3) was added $Zn(CH_3COO)_2 \cdot 2H_2O$ (0.044 g, 0.20 mmol). After the whole was stirred at ambient temperature for 5 h, the resultant fluorescent yellow powder was collected by filtration. X-ray quality crystals of the complex were obtained by recrystallization from a 1:1 mixed solvent of methanol and dichloromethane. Yield = 0.085 g (90% based on Zn). *Anal. Calc.* for $C_{54}H_{40}N_4O_4Zn_2$ ($[Zn_2({}^3CH_2sal)_2]$): C, 69.02; H, 4.29; N, 5.96%. Found: C, 69.05; H, 4.31; N, 5.92%. Characteristic IR data [cm^{-1}]: 1250^m, 1603^s. Diffuse reflectance spectrum [λ_{max} , nm] (relative intensity respect to the 422.0 nm band): 422.0 (1.00), 315.0 (0.92), 238.5 (0.54).

2.9. Synthesis of $[\text{Zn}_2(^2\text{Ssal})_2]$

The complex, $[\text{Zn}_2(^2\text{Ssal})_2]$, was prepared by a slightly modified method for $[\text{Zn}_2(^4\text{Ssal})_2]$, using $^2\text{SsalH}_2$ instead of $^4\text{SsalH}_2$. To a suspension containing $\text{Zn}(\text{CH}_3\text{COO})_2 \cdot 2\text{H}_2\text{O}$ (0.055 g, 0.25 mmol) in methanol (20 cm³) $^2\text{SsalH}_2$ (0.11 g, 0.25 mmol) was added. The mixture was stirred at ambient temperature for 1 h, and then trimethylamine (0.051 g, 0.50 mmol) was added. The whole was stirred for an additional 5 h and followed by addition of dichloromethane (20 cm³). After the resultant fluorescent yellow solution was kept standing at ambient temperature for several days, the grown crystals of the complex were collected by filtration. Yield = 0.097 g (80% based on Zn). *Anal. Calc.* for $\text{C}_{52}\text{H}_{36}\text{N}_4\text{O}_4\text{S}_2\text{Zn}_2$ ($[\text{Zn}_2(^2\text{Ssal})_2]$): C, 64.01; H, 3.72; N, 5.74%. Found: C, 64.05; H, 3.76; N, 5.71%. Characteristic IR data [cm⁻¹]: 1267^m, 1605^s. Diffuse reflectance spectrum [λ_{max} , nm] (relative intensity respect to the 433.0 nm band): 433.0 (1.00), 316.5 (0.90)^{sh}, 238.0 (0.52).

2.10. Crystallographic data collection and structure determination

Single crystals of $[\text{Zn}_2(^4\text{Osal})_2] \cdot 2\text{CH}_2\text{Cl}_2$, $[\text{Zn}_2(^4\text{Ssal})_2] \cdot 3\text{CH}_2\text{Cl}_2$, $[\text{Zn}_2(^3\text{CH}_2\text{sal})_2] \cdot 2\text{CH}_3\text{OH}$, and $[\text{Zn}_2(^2\text{Ssal})_2] \cdot 2\text{CH}_2\text{Cl}_2$ were hand-picked directly out of the reaction mixture in a 1:1 mixed solvent of methanol (or acetonitrile) and dichloromethane, and used for data collection on a Rigaku VariMax Saturn CCD 724 system with graphite-monochromatized MoK α radiation ($\lambda = 0.71075 \text{ \AA}$). The crystal data and experimental parameters are summarized in Table 1. The structures were solved by direct methods and expanded using Fourier techniques [42,43]. The non-hydrogen atoms were refined anisotropically. All the hydrogen atoms were placed in calculated positions and refined with a riding model. For $[\text{Zn}_2(^4\text{Ssal})_2] \cdot 3\text{CH}_2\text{Cl}_2$, there were some solvent molecules were chemically featureless to refine, to solve the issue, the SQUEEZE program implemented PLATON was used to remove contribution of these solvent electron densities, the void volume and void count electrons are 1583 and 408, which indicate the presence of three dichloromethane molecules in the asymmetric unit [44]. The final cycle of full-matrix least-squares refinement on F^2 was based on observed reflections and variable parameters, and converged with unweighted and weighted agreement factors of R and R_w . All calculations were performed using the CrystalStructure crystallographic software package except for refinement, which was performed using SHELXL97 or SHELXL-2018/3 [42,45].

Table 1

Crystallographic data for $[\text{Zn}_2(^4\text{Osal})_2] \cdot 2\text{CH}_2\text{Cl}_2$, $[\text{Zn}_2(^4\text{Ssal})_2] \cdot 3\text{CH}_2\text{Cl}_2$, $[\text{Zn}_2(^3\text{CH}_2\text{sal})_2] \cdot 2\text{CH}_3\text{OH}$, and $[\text{Zn}_2(^2\text{Ssal})_2] \cdot 2\text{CH}_2\text{Cl}_2$.

	$[\text{Zn}_2(^4\text{Osal})_2] \cdot 2\text{CH}_2\text{Cl}_2$	$[\text{Zn}_2(^4\text{Ssal})_2] \cdot 3\text{CH}_2\text{Cl}_2$	$[\text{Zn}_2(^3\text{CH}_2\text{sal})_2] \cdot 2\text{CH}_3\text{OH}$	$[\text{Zn}_2(^2\text{Ssal})_2] \cdot 2\text{CH}_2\text{Cl}_2$
Formula	$\text{C}_{54}\text{H}_{40}\text{Cl}_4\text{N}_4\text{O}_6\text{Zn}_2$	$\text{C}_{55}\text{H}_{42}\text{Cl}_6\text{N}_4\text{O}_4\text{S}_2\text{Zn}_2$	$\text{C}_{56}\text{H}_{48}\text{N}_4\text{O}_6\text{Zn}_2$	$\text{C}_{54}\text{H}_{40}\text{Cl}_4\text{N}_4\text{O}_4\text{S}_2\text{Zn}_2$
Formula weight	1113.51	1230.56	1003.78	1145.63
Crystal size (mm)	0.25 × 0.20 × 0.12	0.24 × 0.24 × 0.20	0.20 × 0.19 × 0.09	0.30 × 0.20 × 0.10
Space group	$P2_1/c$	$P2_1/c$	$P\bar{1}$	$P2_1/c$
a (Å)	17.809(3)	16.076(2)	9.4442(9)	17.096(2)
b (Å)	15.705(2)	19.413(3)	9.9344(10)	31.990(4)
c (Å)	18.245(3)	17.949(3)	12.8426(14)	18.052(2)
α (°)	90	90	76.540(3)	90
β (°)	112.351(3)	93.473(3)	82.389(4)	93.4710(18)
γ (°)	90	90	77.234(4)	90
V (Å ³)	4719.6(13)	5591.3(15)	1138.7(2)	9854(2)
Z	4	4	1	8
Dc (g cm ⁻³)	1.567	1.462	1.464	1.544
μ (cm ⁻¹)	13.010	12.674	11.127	13.273
Trans. factors	0.665–0.855	0.539–0.776	0.736–0.905	0.730–0.876
Tot. reflections	10,802	12,723	5215	22,492
No. of variables	631	577	308	1261
R_1 [$I > 2\sigma(I)$]	0.0420	0.0470	0.0423	0.0860
R (all data)	0.0470	0.0564	0.0430	0.0939
w R_2 (all data)	0.1009	0.1222	0.1323	0.1852
Goodness-of fit on F^2	1.085	1.066	1.113	1.251

2.11. Computational details

All theoretical calculations were performed using the DFT functional B3LYP, as implemented by the GAUSSIAN 16 program package [46–48]. The 6-31G(d,p) basis set was used for the main-group elements, while the LANL2DZ double- ζ quality basis set and effective core potential were applied for the Zn atoms. The singlet ground state (S_0) geometry of each complex was obtained in the gas phase, and then evaluated through calculation of the vibrational frequencies [49–51]. The absence of imaginary frequencies corresponds to the state with minimum energy. The vertical excitation energies at the ground state geometry were obtained from the TD-DFT calculations. GaussView 5.0.9 and Avogadro 1.2.0 were used for data analysis, visualization and surface plots [52,53].

3. Results and discussion

3.1. Crystal structure description of the complexes

An X-ray structural analysis for $[\text{Zn}_2(^4\text{Osal})_2] \cdot 2\text{CH}_2\text{Cl}_2$ revealed the presence of a dinuclear Zn(II) complex molecule and two CH_2Cl_2 molecules of crystallization. A perspective drawing of $[\text{Zn}_2(^4\text{Osal})_2]$ is given in Fig. 1, and its selected bond distances and angles are listed in Table 2 in comparison with those of $[\text{Zn}_2(^4\text{Ssal})_2]$. As shown in Fig. 1, each Zn(II) center in $[\text{Zn}_2(^4\text{Osal})_2]$ is coordinated by two NO chelating sites from two different $^4\text{Osal}^{2-}$ ligands. The dihedral angle between two ZnNO planes in each Zn(II) center is 71.030° for Zn1 and 80.812° for Zn2, indicating a distorted tetrahedral geometry. Such a slight deviation from the ideal tetrahedron is considered to originate from the moderate rigidity of the ligand. The averaged dihedral angle between the two aniline frameworks in the coordinated ligand is 80.33(7)°, reflecting that the O5 or O6 atom, that acts as a torsion-generating source, takes a tetrahedral geometry. On the other hand, the averaged interplane angle between the aniline framework and the salicylaldehyde moiety is 48.85(7)°. This implies that these two adjacent moieties are not coplanar and hence the ligand possesses reasonable flexibility. As a result, the two ligands in $[\text{Zn}_2(^4\text{Osal})_2]$ can intersect each other along the intramolecular Zn-Zn axis to afford a double-stranded helical structure. The Zn-Zn separation (11.564(2) Å) in $[\text{Zn}_2(^4\text{Osal})_2]$ is shorter than that (11.724(3) Å) in $[\text{Zn}_2(^4\text{CH}_2\text{sal})_2]$ [24]. This implies that the torsion generating source in the ligand affects the overall structure of the complex. Although $[\text{Zn}_2(^4\text{Ssal})_2]$ takes a similar double-stranded helical dinuclear structure to $[\text{Zn}_2(^4\text{Osal})_2]$ (Fig. 1), the

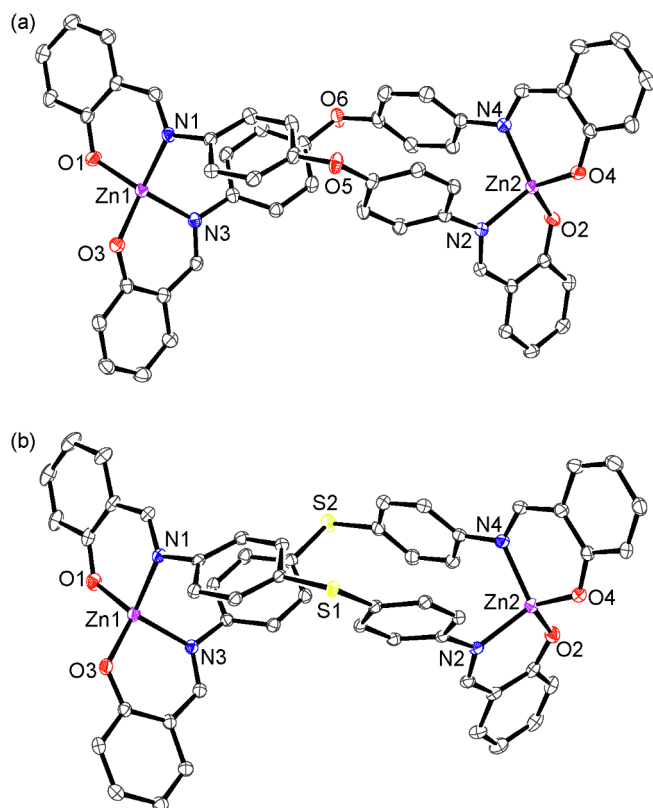


Fig. 1. Perspective views of $[\text{Zn}_2(^4\text{Osald})_2]$ (a) and $[\text{Zn}_2(^4\text{Ssal})_2]$ (b) with the atomic labeling schemes (50% probability ellipsoids for $[\text{Zn}_2(^4\text{Osald})_2]$ and 25% probability ellipsoids for $[\text{Zn}_2(^4\text{Ssal})_2]$).

Table 2
Selected bond distances (Å) and angles (deg) for $[\text{Zn}_2(^4\text{Osald})_2] \cdot 2\text{CH}_2\text{Cl}_2$ and $[\text{Zn}_2(^4\text{Ssal})_2] \cdot 3\text{CH}_2\text{Cl}_2$.

	$[\text{Zn}_2(^4\text{Osald})_2] \cdot 2\text{CH}_2\text{Cl}_2$	$[\text{Zn}_2(^4\text{Ssal})_2] \cdot 3\text{CH}_2\text{Cl}_2$
Zn1-O1	1.917(2)	1.908(2)
Zn1-O3	1.9130(15)	1.9023(19)
Zn1-N1	2.018(2)	2.016(2)
Zn1-N3	2.026(2)	2.009(2)
Zn2-O2	1.9121(15)	1.915(2)
Zn2-O4	1.913(2)	1.908(2)
Zn2-N2	2.007(2)	2.004(2)
Zn2-N4	2.0120(19)	2.022(2)
O1-Zn1-O3	108.20(8)	115.59(8)
O1-Zn1-N1	94.97(8)	95.70(8)
O1-Zn1-N3	128.07(7)	122.31(9)
O3-Zn1-N1	130.22(7)	124.54(8)
O3-Zn1-N3	95.39(7)	96.57(8)
N1-Zn1-N3	104.03(9)	103.77(9)
O2-Zn2-O4	116.00(8)	116.26(9)
O2-Zn2-N2	96.53(8)	96.59(9)
O2-Zn2-N4	124.05(7)	124.15(9)
O4-Zn2-N2	119.59(7)	121.72(9)
O4-Zn2-N4	96.30(8)	96.73(9)
N2-Zn2-N4	105.73(9)	102.65(9)

difference with 0.094° between the dihedral angles around two Zn centers (78.406° for Zn1 and 78.312° for Zn2) in $[\text{Zn}_2(^4\text{Ssal})_2]$ is considerably smaller than that (9.782°) in $[\text{Zn}_2(^4\text{Osald})_2]$. In contrast to these dihedral angles, the difference with $24.50(8)^\circ$ between the dihedral angles around two torsion generating sources ($61.19(7)^\circ$ for S1 and $85.69(8)^\circ$ for S2) in $[\text{Zn}_2(^4\text{Ssal})_2]$ is significantly larger than that ($6.47(7)^\circ$) in $[\text{Zn}_2(^4\text{Osald})_2]$. On the other hand, the averaged interplane angle between the aniline framework and the salicylaldimine moiety in $[\text{Zn}_2(^4\text{Ssal})_2]$ is $42.88(8)^\circ$, which is somewhat acute than the

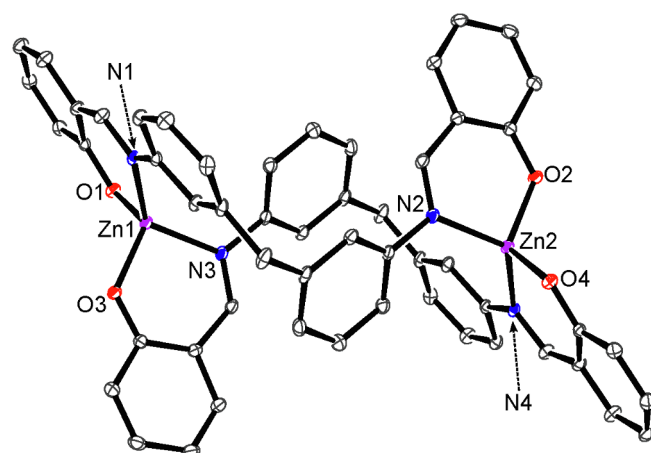


Fig. 2. Perspective view of $[\text{Zn}_2(^3\text{CH}_2\text{sal})_2]$ with the atomic labeling scheme (50% probability ellipsoids).

corresponding angle ($48.85(7)^\circ$) in $[\text{Zn}_2(^4\text{Osald})_2]$. Furthermore, the Zn-Zn separation with $11.361(1) \text{ \AA}$ in $[\text{Zn}_2(^4\text{Ssal})_2]$ is shorter than those in $[\text{Zn}_2(^3\text{CH}_2\text{sal})_2]$ ($11.564(2) \text{ \AA}$) and $[\text{Zn}_2(^4\text{CH}_2\text{sal})_2]$ ($11.724(3) \text{ \AA}$) [24]. No significant difference can be recognized for the bond distances and angles around the Zn(II) centers between these three complexes. These facts reflect differences of the torsion generating sources in the complexes.

Similarly to the cases of $^4\text{CH}_2\text{sal}^{2-}$, $^4\text{Osald}^{2-}$, and $^4\text{Ssal}^{2-}$ derived from the 4,4'-precursors, the N_2O_2 ligand $^3\text{CH}_2\text{sal}^{2-}$ derived from bis(3-aminophenyl)methane affords a dinuclear complex formulated as $[\text{Zn}_2(^3\text{CH}_2\text{sal})_2]$. As shown in Fig. 2, each Zn(II) center in $[\text{Zn}_2(^3\text{CH}_2\text{sal})_2]$ is coordinated by two NO chelating sites from two different $^3\text{CH}_2\text{sal}^{2-}$ ligands. There is no apparent difference in bonding distances and angles around the Zn(II) centers in the complex when comparing with $[\text{Zn}_2(^4\text{CH}_2\text{sal})_2]$ (Table 3) [24]. The dihedral angle between two ZnNO planes in each Zn(II) center is 82.176° , indicating a similar distorted tetrahedral geometry to $[\text{Zn}_2(^4\text{Osald})_2]$ and $[\text{Zn}_2(^4\text{Ssal})_2]$ derived from 4,4'-precursors. On the other hand, the dihedral angle around the torsion generating source in $[\text{Zn}_2(^3\text{CH}_2\text{sal})_2]$ ($90.96(5)^\circ$) is closer to the ideal angle (90°) than the corresponding angles in $[\text{Zn}_2(^4\text{Osald})_2]$ and $[\text{Zn}_2(^4\text{Ssal})_2]$. The averaged interplane angle between the aniline framework and the salicylaldimine moiety in $[\text{Zn}_2(^3\text{CH}_2\text{sal})_2]$ is $22.26(6)^\circ$, which is somewhat acute than the corresponding angle in $[\text{Zn}_2(^4\text{Osald})_2]$ ($48.85(7)^\circ$) and $[\text{Zn}_2(^4\text{Ssal})_2]$ ($42.88(8)^\circ$). Furthermore, the Zn-Zn separation with $8.6090(8) \text{ \AA}$ in $[\text{Zn}_2(^3\text{CH}_2\text{sal})_2]$ is obviously shorter than those in $[\text{Zn}_2(^4\text{CH}_2\text{sal})_2]$ ($11.724(3) \text{ \AA}$), $[\text{Zn}_2(^4\text{Osald})_2]$ ($11.564(2) \text{ \AA}$), and $[\text{Zn}_2(^4\text{Ssal})_2]$ ($11.361(1) \text{ \AA}$) [24]. Although two absolute configurations, Δ and Λ , are possible for each Zn(II) center in $[\text{Zn}_2(^3\text{CH}_2\text{sal})_2]$, the configurations

Table 3
Selected bond distances (Å) and angles (deg) for $[\text{Zn}_2(^3\text{CH}_2\text{sal})_2] \cdot 2\text{CH}_3\text{OH}$.

	$[\text{Zn}_2(^3\text{CH}_2\text{sal})_2] \cdot 2\text{CH}_3\text{OH}$
Zn1-O1	1.9185(13)
Zn1-O2 ^{a)}	1.9205(16)
Zn1-N1	2.0016(15)
Zn1-N2 [*]	2.0011(17)
O1-Zn1-O2 [*]	117.98(7)
O1-Zn1-N1	98.13(6)
O1-Zn1-N2 [*]	110.09(6)
O2 [*] -Zn1-N1	111.64(6)
O2 [*] -Zn1-N2 [*]	96.75(7)
N1-Zn1-N2 [*]	123.72(7)

a) Symmetry codes for atoms with asterisks: $-x + 1, -y + 1, -z + 1$.

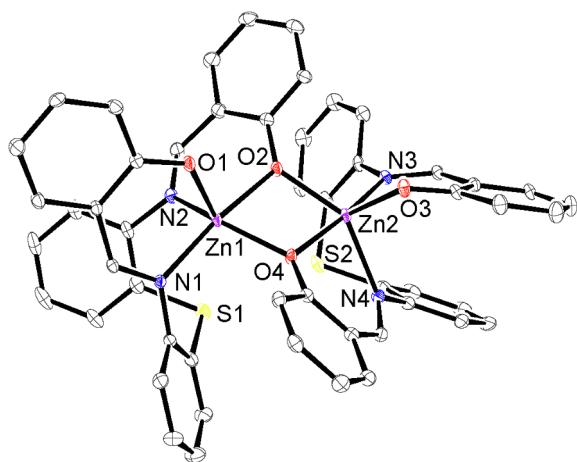


Fig. 3. Perspective view of $[\text{Zn}_2(^2\text{Ssal})_2]$ with the atomic labeling scheme (50% probability ellipsoids).

Table 4
Selected bond distances (Å) and angles (deg) for $[\text{Zn}_2(^2\text{Ssal})_2]\cdot 2\text{CH}_2\text{Cl}_2$.

	$[\text{Zn}_2(^2\text{Ssal})_2]\cdot 2\text{CH}_2\text{Cl}_2$	
	Molecule A	Molecule B
Zn1-O1 (Zn3-O5)	1.971(3)	1.973(3)
Zn1-O2 (Zn3-O6)	2.072(3)	2.064(3)
Zn1-O4 (Zn3-O8)	2.036(3)	2.021(3)
Zn1-N1 (Zn3-N5)	2.115(4)	2.114(4)
Zn1-N2 (Zn3-N6)	2.123(4)	2.132(4)
Zn2-O2 (Zn4-O6)	2.014(3)	2.015(3)
Zn2-O3 (Zn4-O7)	1.964(3)	1.953(3)
Zn2-O4 (Zn4-O8)	2.070(3)	2.073(3)
Zn2-N3 (Zn4-N7)	2.106(4)	2.117(4)
Zn2-N4 (Zn4-N8)	2.140(4)	2.129(4)
O1-Zn1-O2 (O5-Zn3-O6)	95.76(13)	98.12(13)
O1-Zn1-O4 (O5-Zn3-O8)	112.62(13)	110.84(13)
O1-Zn1-N1 (O5-Zn3-N5)	90.00(13)	89.03(14)
O1-Zn1-N2 (O5-Zn3-N6)	101.12(13)	101.89(14)
O2-Zn1-O4 (O6-Zn3-O8)	75.76(12)	75.94(12)
O2-Zn1-N1 (O6-Zn3-N5)	173.20(13)	172.78(14)
O2-Zn1-N2 (O6-Zn3-N6)	83.57(14)	83.30(14)
O4-Zn1-N1 (O8-Zn3-N5)	98.69(13)	100.58(13)
O4-Zn1-N2 (O8-Zn3-N6)	141.70(14)	143.16(14)
N1-Zn1-N2 (N5-Zn3-N6)	98.89(14)	96.31(15)
O2-Zn2-O3 (O6-Zn4-O7)	114.12(13)	114.05(13)
O2-Zn2-O4 (O6-Zn4-O8)	76.28(12)	75.89(12)
O2-Zn2-N3 (O6-Zn4-N7)	97.16(14)	96.49(13)
O2-Zn2-N4 (O6-Zn4-N8)	145.44(14)	144.78(14)
O3-Zn2-O4 (O7-Zn4-O8)	101.49(13)	99.43(13)
O3-Zn2-N3 (O7-Zn4-N7)	89.40(14)	90.16(14)
O3-Zn2-N4 (O7-Zn4-N8)	97.08(14)	97.35(14)
O4-Zn2-N3 (O8-Zn4-N7)	168.85(13)	169.55(13)
O4-Zn2-N4 (O8-Zn4-N8)	83.51(13)	83.90(14)
N3-Zn2-N4 (N7-Zn4-N8)	97.68(14)	99.06(14)

around Zn1 and Zn1* are stereoselectively unified to Λ and Δ , respectively. This implies that $[\text{Zn}_2(^3\text{CH}_2\text{sal})_2]$ adopts a dinuclear mesocate structure. These facts suggest that structural characteristics of such complexes depend on the relative arrangement of the two amino groups in the precursor dianiline.

In the crystal of $[\text{Zn}_2(^2\text{Ssal})_2]\cdot 2\text{CH}_2\text{Cl}_2$, which consists of two independent neutral complexes, their structures are almost the same as each other, and hence only one complex molecule is shown in Fig. 3 (Table 4). As seen from Fig. 3, $[\text{Zn}_2(^2\text{Ssal})_2]$ has a unique structure entirely different from the dinuclear helicates, $[\text{Zn}_2(^4\text{CH}_2\text{sal})_2]$, $[\text{Zn}_2(^4\text{Osai})_2]$, and $[\text{Zn}_2(^4\text{Osai})_2]$, as well as the mesocate, $[\text{Zn}_2(^3\text{CH}_2\text{sal})_2]$. In $[\text{Zn}_2(^2\text{Ssal})_2]$, for instance, each Zn(II) center is coordinated by two NO chelating sites from the same $^2\text{Ssal}^{2-}$ ligand,

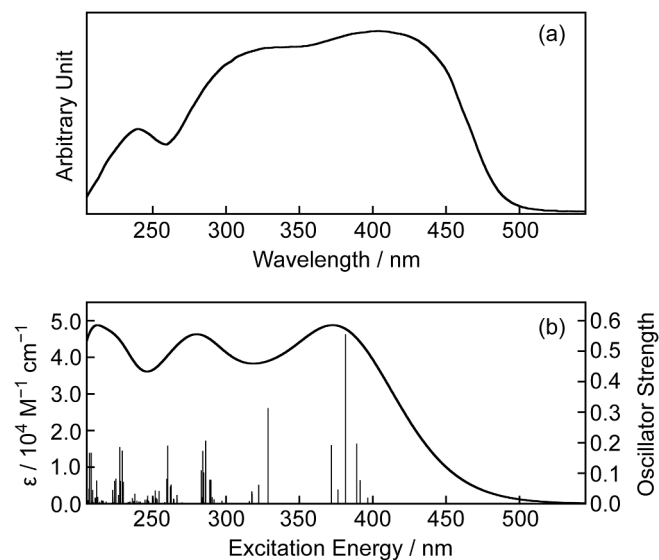


Fig. 4. Diffuse reflectance spectra of $[\text{Zn}_2(^4\text{Osai})_2]$ (a) and the estimated spectrum for photo-absorption processes in $[\text{Zn}_2(^4\text{Osai})_2]$ by the TD-DFT calculations.

and one of the coordinated O^- donors bridges another Zn(II) center to form a doubly phenoxo-bridged dinuclear structure. Although each Zn(II) center apparently takes a 5-coordinated geometry, the sulfur atom of $^2\text{Ssal}^{2-}$ is located at a distance of avg. 3.0368(8) Å in the vicinity of the 6th coordination site. The Zn-Zn separation with avg. 3.1863(8) Å in $[\text{Zn}_2(^2\text{Ssal})_2]$ is close enough to not compare with other complexes, $[\text{Zn}_2(^4\text{CH}_2\text{sal})_2]$, $[\text{Zn}_2(^4\text{Osai})_2]$, $[\text{Zn}_2(^4\text{Ssal})_2]$, and $[\text{Zn}_2(^3\text{CH}_2\text{sal})_2]$. These structural features can be attributed to the fact that the relative positions of two amino groups in the precursor are very close.

3.2. Characterization

The complexes, $[\text{Zn}_2(^4\text{Osai})_2]$, $[\text{Zn}_2(^4\text{Ssal})_2]$, $[\text{Zn}_2(^3\text{CH}_2\text{sal})_2]$, and $[\text{Zn}_2(^2\text{Ssal})_2]$ were readily prepared by the reactions of Zn $(\text{CH}_3\text{COO})_2\cdot 2\text{H}_2\text{O}$ with $^4\text{OsaiH}_2$, $^4\text{SsalH}_2$, $^3\text{CH}_2\text{salH}_2$, and $^2\text{SsalH}_2$, respectively, in the presence of appropriate base. These complexes crystallize as yellow crystals with CH_2Cl_2 or CH_3OH molecules. These molecules of crystallization in $[\text{Zn}_2(^4\text{Osai})_2]\cdot 2\text{CH}_2\text{Cl}_2$, $[\text{Zn}_2(^4\text{Ssal})_2]\cdot 3\text{CH}_2\text{Cl}_2$, $[\text{Zn}_2(^3\text{CH}_2\text{sal})_2]\cdot 2\text{CH}_3\text{OH}$, and $[\text{Zn}_2(^2\text{Ssal})_2]\cdot 2\text{CH}_2\text{Cl}_2$ are easily lost when the crystal is exposed to air for a long time. In the solid state, however, each complex itself is stable over several months. Each of the N_2O_2 ligands, $^4\text{CH}_2\text{salH}_2$, $^4\text{OsaiH}_2$, $^4\text{SsalH}_2$, $^3\text{CH}_2\text{salH}_2$, and $^2\text{SsalH}_2$, has two equivalent azomethine groups, while the corresponding complex has four undistinguishable azomethine groups. In the infrared spectrum, actually, $[\text{Zn}_2(^4\text{Osai})_2]$ ($^4\text{OsaiH}_2$) shows only single band due to the imine $\text{C}=\text{N}$ stretching vibration at 1604 cm^{-1} (1608 cm^{-1}). Similar to the case of $[\text{Zn}_2(^4\text{Osai})_2]$, only single band can be observed around 1600 cm^{-1} for $[\text{Zn}_2(^4\text{CH}_2\text{sal})_2]$ (1610 cm^{-1}), $[\text{Zn}_2(^4\text{Ssal})_2]$ (1601 cm^{-1}), $[\text{Zn}_2(^3\text{CH}_2\text{sal})_2]$ (1603 cm^{-1}), and $[\text{Zn}_2(^2\text{Ssal})_2]$ (1604 cm^{-1}). It should be noted that these bands for the complexes appear in the lower-wave-number sides compared with the corresponding bands for the ligands (1614 cm^{-1} for $^4\text{CH}_2\text{salH}_2$, 1608 cm^{-1} for $^4\text{SsalH}_2$, 1618 cm^{-1} for $^3\text{CH}_2\text{salH}_2$, and 1610 cm^{-1} for $^2\text{SsalH}$) [54–59]. These shifts indicate that the ligands coordinate to the zinc(II) centres through the imine nitrogen atoms. Although the ligands, $^4\text{CH}_2\text{salH}_2$, $^4\text{OsaiH}_2$, $^4\text{SsalH}_2$, $^3\text{CH}_2\text{salH}_2$, and $^2\text{SsalH}_2$, exhibit broad bands around 2700 cm^{-1} due to the intramolecular hydrogen-bonded phenol $\text{O}-\text{H}$ stretching vibration, the corresponding bands cannot be seen in the spectra of the complexes, $[\text{Zn}_2(^4\text{CH}_2\text{sal})_2]$, $[\text{Zn}_2(^4\text{Osai})_2]$, $[\text{Zn}_2(^4\text{Ssal})_2]$, $[\text{Zn}_2(^3\text{CH}_2\text{sal})_2]$, and $[\text{Zn}_2(^2\text{Ssal})_2]$ [56,57]. In the case of the complexes, furthermore, the bands due to the phenol $\text{C}-\text{O}$ stretching vibration are shifted to the

Table 5

Selected vertical singlet excitations with the lowest energy or higher intensities ($f > 0.1$) for $[\text{Zn}_2(^4\text{Msal})_2]$ from TD-DFT calculations at the S_0 geometry.

State	Calculated			Observed ^a	
	λ [nm]	Oscillator strength (f)	Main contributor	λ [nm]	Relative intensity ^b
S ₁	392.43	0.0107	HOMO→LUMO (67.0%)	418.0	1.00
S ₃	387.90	0.1399	HOMO-1→LUMO (62.7%)		
S ₅	382.01	0.5008	HOMO→LUMO+2 (61.8%)		
S ₈	371.39	0.2678	HOMO-3→LUMO+2 (44.6%) HOMO-1→LUMO+3 (44.1%)		
S ₁₇	320.35	0.4061	HOMO-5→LUMO (63.3%)	319.5	0.91
S ₁₈	319.93	0.2679	HOMO-4→LUMO (61.8%)		
S ₂₀	314.02	0.1186	HOMO-4→LUMO+1 (53.6%)		
S ₃₂	289.48	0.1466	HOMO-7→LUMO+1 (76.6%)		
S ₃₄	286.77	0.1439	HOMO-6→LUMO+3 (83.6%)		
S ₃₅	286.06	0.1625	HOMO-7→LUMO+2 (59.0%)		
S ₃₆	285.95	0.1390	HOMO-7→LUMO+3 (80.6%)	238.0	0.48
S ₁₂₁	227.73	0.2645	HOMO-2→LUMO+13 (36.9%) HOMO→LUMO+12 (52.4%)		
S ₁₂₄	225.97	0.1118	HOMO-7→LUMO+6 (23.8%) HOMO-6→LUMO+5 (27.8%) HOMO-3→LUMO+13 (15.5%)		
S ₁₂₉	225.21	0.1248	HOMO-1→LUMO+12 (24.4%) HOMO-2→LUMO+15 (32.2%) HOMO→LUMO+14 (49.2%)		

^a In the crystalline state.

^b Respect to the 418.0 nm band.

Table 6

Selected vertical singlet excitations with the lowest energy or higher intensities ($f > 0.1$) for $[\text{Zn}_2(^4\text{OsAl})_2]$ from TD-DFT calculations at the S_0 geometry.

State	Calculated			Observed ^a	
	λ [nm]	Oscillator strength (f)	Main contributor	λ [nm]	Relative intensity ^b
S ₁	396.48	0.0198	HOMO→LUMO (72.0%)	419.0	1.00
S ₃	388.95	0.1970	HOMO-1→LUMO (67.8%)		
S ₅	381.33	0.5555	HOMO→LUMO+2 (65.5%)		
S ₈	371.78	0.1922	HOMO-3→LUMO+2 (39.7%) HOMO-1→LUMO+3 (55.7%)		
S ₁₇	328.56	0.3133	HOMO-5→LUMO (83.6%)	316 ^{sh}	0.90
S ₁₈	328.53	0.1896	HOMO-4→LUMO (83.4%)		
S ₃₇	286.03	0.2064	HOMO-6→LUMO+3 (59.4%)		
S ₃₉	284.66	0.1029	HOMO-1→LUMO+5 (81.1%)		
S ₄₁	284.06	0.1735	HOMO-7→LUMO+3 (77.9%)		
S ₄₃	283.07	0.1093	HOMO-7→LUMO+2 (39.9%) HOMO-2→LUMO+5 (26.7%)		
S ₆₀	260.05	0.1904	HOMO-1→LUMO+8 (36.2%)	239.0	0.47
S ₁₂₆	229.08	0.1742	HOMO-5→LUMO+8 (66.9%)		
S ₁₂₈	227.42	0.1861	HOMO-2→LUMO+13 (21.7%) HOMO→LUMO+12 (39.7%)		

^a In the crystalline state.

^b Respect to the 419.0 nm band.

^{sh} The 'sh' denotes a shoulder.

lower-energy side and appear at 1256 cm^{-1} for $[\text{Zn}_2(^4\text{CH}_2\text{sal})_2]$, 1256 cm^{-1} for $[\text{Zn}_2(^4\text{OsAl})_2]$, 1252 cm^{-1} for $[\text{Zn}_2(^4\text{Ssal})_2]$, 1250 cm^{-1} for $[\text{Zn}_2(^3\text{CH}_2\text{sal})_2]$, and 1267 cm^{-1} for $[\text{Zn}_2(^2\text{Ssal})_2]$ in comparison with the corresponding bands of ligands [54,55]. These implies that the ligands coordinate to the zinc(II) centres through the phenolate oxygen atoms. In the region lower than 600 cm^{-1} , the spectra of $[\text{Zn}_2(^4\text{CH}_2\text{sal})_2]$, $[\text{Zn}_2(^4\text{OsAl})_2]$, $[\text{Zn}_2(^4\text{Ssal})_2]$, $[\text{Zn}_2(^3\text{CH}_2\text{sal})_2]$, and

$[\text{Zn}_2(^2\text{Ssal})_2]$ exhibit some additional bands, which are not observed for $^4\text{CH}_2\text{salH}_2$, $^4\text{OsAlH}_2$, $^4\text{SsalH}_2$, $^3\text{CH}_2\text{salH}_2$, and $^2\text{SsalH}_2$. These facts also support the structures determined by single crystal X-ray structural analyses.

Diffuse reflectance spectra of all complexes are roughly composed of three bands. As a representative example, the spectrum of $[\text{Zn}_2(^4\text{OsAl})_2]$ is shown in Fig. 4. The complex, $[\text{Zn}_2(^4\text{OsAl})_2]$, shows two peaks at

Table 7
Selected vertical singlet excitations with the lowest energy or higher intensities ($f > 0.1$) for $[\text{Zn}_2(^4\text{Ssal})_2]$ from TD-DFT calculations at the S_0 geometry.

State	λ [nm]	Calculated		Observed ^a	
		Oscillator strength (f)	Main contributor	λ [nm]	Relative intensity ^b
S ₁	395.79	0.0314	HOMO→LUMO (78.7%)	422.5	1.00
S ₂	389.26	0.3265	HOMO-1→LUMO (76.8%)		
S ₅	382.42	0.4096	HOMO→LUMO+2 (79.4%)		
S ₈	368.90	0.2815	HOMO-3→LUMO+2 (37.5%)		
			HOMO-1→LUMO+3 (53.2%)		
S ₁₇	337.82	0.1788	HOMO-4→LUMO (89.0%)		
S ₁₈	336.85	0.1064	HOMO-5→LUMO (87.0%)		
S ₃₁	285.47	0.1485	HOMO-6→LUMO+1 (80.2%)		
S ₃₂	285.15	0.1602	HOMO-7→LUMO+1 (62.8%)		
S ₃₃	284.69	0.1032	HOMO-7→LUMO+1 (24.7%)		
			HOMO→LUMO+4 (47.5%)		
S ₃₅	281.83	0.2229	HOMO-6→LUMO+3 (84.6%)		
S ₃₉	280.37	0.1964	HOMO-7→LUMO+3 (86.8%)		
S ₄₀	279.90	0.2131	HOMO-7→LUMO+2 (58.0%)	238.5	0.55
S ₁₃₄	227.14	0.2470	HOMO→LUMO+12 (56.8%)		

^a In the crystalline state.

^b Respect to the 422.5 nm band.

^{sh} The 'sh' denotes a shoulder.

419.0 and 239.0 nm, and one shoulder at 316 nm. The corresponding three bands slightly shift toward the shorter- or longer-wavelength side in the spectrum of $[\text{Zn}_2(^4\text{Ssal})_2]$ (Fig. S1), indicating that types of torsion-generating sources influence the electronic states of the complexes. Similarly, the spectral difference between $[\text{Zn}_2(^3\text{CH}_2\text{sal})_2]$ and $[\text{Zn}_2(^4\text{CH}_2\text{sal})_2]$ suggests that even in the case of the complexes consisting of the ligands with the same torsion-generating sources, the electronic states differ from each other if the spatial separations of the two coordination sites are distinguishable from each other (Figs. S2 and S3). Although $[\text{Zn}_2(^2\text{Ssal})_2]$ shows a similar spectrum to the other four complexes, the peak with the lowest energy appears on the longer-wavelength side than the other complexes (Fig. S4). These differences suggest that the electronic states differ considerably between the phenoxo-bridged dinuclear complex ($[\text{Zn}_2(^2\text{Ssal})_2]$) and the dinuclear helicate ($[\text{Zn}_2(^4\text{CH}_2\text{sal})_2]$, $[\text{Zn}_2(^4\text{OsSal})_2]$, $[\text{Zn}_2(^4\text{Ssal})_2]$) or mesocate complex ($[\text{Zn}_2(^3\text{CH}_2\text{sal})_2]$).

The above experimental results for photo-absorption processes are summarized in Tables 5–9, compared with the TD-DFT calculations. For all the complexes, as shown in Figs. 4, S1 – S4, the simulated spectra from the TD-DFT calculations relatively correspond well with the observed bands in the diffuse reflectance spectra. In each complex, all the observed bands are due to the overlaps of plural calculated electronic transitions. In the case of diffuse reflectance spectrum of $[\text{Zn}_2(^4\text{CH}_2\text{sal})_2]$, for instance, the 418.0 nm band is due to the overlap of the relatively intense $S_0 \rightarrow S_3$, $S_0 \rightarrow S_5$, and $S_0 \rightarrow S_8$ transitions (Table 5). The calculation also indicates that the lowest singlet excited state (S_1) exists around the edge of the 418.0 nm band. It is reasonable to know the nature of the $S_0 \rightarrow S_1$ transition for each complex, as the S_1 state plays an important role in the photoluminescence process described later. The isosurfaces in electron densities of the selected molecular orbitals are depicted in Fig. 5–9 and S5 – S9, and the compositions of the molecular orbitals from atomic orbital contributions are also given in Tables 5–9. In the case of $[\text{Zn}_2(^4\text{CH}_2\text{sal})_2]$, as shown in Table 5, the main contributor for the S_1 state is the electronic configuration corresponding to the excitation from the highest occupied molecular orbital (HOMO) to the lowest unoccupied molecular orbital (LUMO). Among these orbitals, HOMO is a localized molecular orbital on four terminal phenolate moieties (Fig. 5). On the other hand, LUMO is a molecular orbital localized mainly on four terminal imonophenyl

groups. It can be regarded therefore that the $S_0 \rightarrow S_1$ transition has an intramolecular charge-transfer (CT) character from the oxide groups to the imino groups in the terminal salicylaldehyde moieties of the coordinated $^4\text{CH}_2\text{sal}^{2-}$ ligands. Similar to the case of $[\text{Zn}_2(^4\text{CH}_2\text{sal})_2]$, the S_1 states of $[\text{Zn}_2(^4\text{OsSal})_2]$ and $[\text{Zn}_2(^4\text{Ssal})_2]$ are contributed mainly by the excitations from HOMOs to LUMOs. In $[\text{Zn}_2(^4\text{OsSal})_2]$, however, electron densities are distributed slightly on the non-bonding orbitals of the ether-oxygen atoms in HOMO, while those are distributed not on the non-bonding orbitals but on the central phenylimino groups in LUMO. Accordingly, the S_1 state of $[\text{Zn}_2(^4\text{OsSal})_2]$ has some $n\pi^*$ character in the central bis(4-phenyl)ether moieties. Such a distribution of electron densities on the non-bonding orbitals in HOMO is enhanced in the thioether-sulfur atoms of $[\text{Zn}_2(^4\text{Ssal})_2]$, indicating that its S_1 state has a stronger $n\pi^*$ character than that of $[\text{Zn}_2(^4\text{OsSal})_2]$. In the case of $[\text{Zn}_2(^2\text{Ssal})_2]$, on the other hand, the main contributor is HOMO \rightarrow LUMO. Although HOMO is localized molecular orbital on the salicylaldehyde moieties containing the non-bridging oxide groups, LUMO is localized molecular orbital the remaining two salicylaldehyde moieties containing the bridging oxide groups. This indicates that the S_1 state of the complex has a unique CT character between the two different kinds of salicylaldehyde moieties.

In the solid-state photoluminescence spectra, all the complexes show single emission bands in the 450–550 nm region (Figs. 10, S10 – S13). As a representative example, the spectrum of $[\text{Zn}_2(^4\text{OsSal})_2]$ is shown in Fig. 10, together with its excitation spectrum. The photoluminescence spectrum of $[\text{Zn}_2(^4\text{OsSal})_2]$ exhibits a single band at 506.0 nm upon excitation by the UV light. The yellowish green luminescence of the complex can be also observed in an air-saturated solution, and hence seems to be due to the fluorescence from its S_1 state. Actually, the luminescence and excitation spectra of the complex have a good mirror image relationship, and its Stokes shift is relatively small (1.79 kcm^{-1}). It can be concluded therefore that the luminescence is assigned as the $\pi\text{-}\pi^*$ transition localized mainly on the coordinated $^4\text{OsSal}^{2-}$ ligands. The Stokes shift of $[\text{Zn}_2(^4\text{OsSal})_2]$ is larger than that of the free ligand, $^4\text{OsSalH}_2$, and similar trends are also observed for the other complexes and ligands (Table 10). Despite being complexes containing similar 4,4'-dianiline-derived ligands, as shown in Table 10, $[\text{Zn}_2(^4\text{CH}_2\text{sal})_2]$ and $[\text{Zn}_2(^4\text{Ssal})_2]$ show excitation and emission maxima with slightly different energies from those of $[\text{Zn}_2(^4\text{OsSal})_2]$.

Table 8
Selected vertical singlet excitations with the lowest energy or higher intensities ($f > 0.1$) for $[\text{Zn}_2(^3\text{Msal})_2]$ from TD-DFT calculations at the S_0 geometry.

State	λ [nm]	Calculated		Observed ^a			
		Oscillator strength (f)	Main contributor	λ [nm]	Relative intensity ^b		
S ₁	396.02	0.0000	HOMO-1→LUMO+1 (29.1%) HOMO→LUMO (56.6%)	422.0	1.00		
S ₄	391.75	0.1549	HOMO-3→LUMO (67.4%)				
S ₆	379.36	0.2271	HOMO→LUMO+1 (34.6%) HOMO→LUMO+2 (39.1%)				
S ₁₀	376.02	0.2135	HOMO-2→LUMO+1 (25.8%) HOMO-2→LUMO+2 (42.2%)				
S ₁₂	372.86	0.1243	HOMO-2→LUMO+1 (26.3%) HOMO-1→LUMO+3 (21.7%) HOMO→LUMO+1 (23.0%)				
S ₁₈	313.95	0.1401	HOMO-4→LUMO (52.8%)			315.0	0.92
S ₂₀	310.16	0.2601	HOMO-6→LUMO (23.6%) HOMO-4→LUMO (18.2%)				
S ₃₀	292.49	0.1022	HOMO-7→LUMO+2 (29.6%) HOMO-5→LUMO+2 (41.8%)				
S ₃₁	291.66	0.2279	HOMO-12→LUMO (10.4%) HOMO-10→LUMO (10.0%) HOMO-5→LUMO+1 (13.4%) HOMO-4→LUMO+3 (22.2%)				
S ₃₄	288.01	0.5363	HOMO-9→LUMO+2 (7.4%) HOMO-8→LUMO (8.2%) HOMO-7→LUMO+1 (12.0%) HOMO-7→LUMO+2 (13.3%) HOMO-6→LUMO+3 (11.3%) HOMO-4→LUMO+3 (14.9%)				
S ₁₂₂	226.76	0.1560	HOMO-1→LUMO+13 (43.4%) HOMO→LUMO+12 (30.6%)	238.5	0.54		
S ₁₂₃	226.33	0.1640	HOMO-3→LUMO+13 (26.2%) HOMO-2→LUMO+12 (34.1%) HOMO→LUMO+12 (33.6%)				
S ₁₂₅	225.17	0.1298	HOMO-2→LUMO+12 (18.6%) HOMO-1→LUMO+15 (34.0%) HOMO→LUMO+14 (20.5%)				

^a In the crystalline state.

^b Respect to the 422.0 nm band.

Furthermore, fluorescence lifetimes and quantum yields also differ from one another among these three complexes (Table 10). These facts show that the torsion-generating sources affect nature of electronic transitions of the complexes, and are essentially consistent with the results of the above mentioned TD-DFT calculations. On the other hand, the emission maximum, lifetime, and quantum yield of $[\text{Zn}_2(^3\text{CH}_2\text{sal})_2]$ differ from those of $[\text{Zn}_2(^4\text{CH}_2\text{sal})_2]$ with the same composition, indicating that the structures of the ligands and/or complexes affect their photoluminescence properties. As expected from the dinuclear structures with distinctly different bridging modes, the luminescent properties of $[\text{Zn}_2(^2\text{Ssal})_2]$ are distinguishable from those of $[\text{Zn}_2(^4\text{Ssal})_2]$. Namely, the excitation and emission maxima of $[\text{Zn}_2(^4\text{Ssal})_2]$ are located at 472.0 and 511.0 nm, respectively, and the corresponding maxima of $[\text{Zn}_2(^2\text{Ssal})_2]$ shift toward the longer-wavelength side and appear at 481.0 and 520.0 nm, respectively. This implies that the relative position of the two amino groups of the precursor dianiline have a great effect on not only the structure of the complex but the electronic state.

4. Conclusion

Four dinuclear zinc(II) complexes with N_2O_2 ligands, bis(*N*-salicylidene)-4,4'-diaminodiphenyl)ether (⁴OsalH₂), bis(*N*-salicylidene)-4,4'-diaminodiphenyl)thioether (⁴SsalH₂), bis(*N*-salicylidene)-3,3'-diaminodiphenyl)methane (³CH₂salH₂), and bis(*N*-salicylidene)-2,2'-diaminodiphenyl)thioether (²SsalH₂), have been newly prepared and characterized by some spectroscopic methods and single-crystal X-ray diffraction together with DFT calculations. The ligands (⁴OsalH₂ and ⁴SsalH₂) derived from 4,4'-dianiline afford similar helical dinuclear complexes ($[\text{Zn}_2(^4\text{Osal})_2]$ and $[\text{Zn}_2(^4\text{Ssal})_2]$) to the already reported complex with bis(*N*-salicylidene)-4,4'-diaminodiphenyl)methane (⁴CH₂salH₂), $[\text{Zn}_2(^4\text{CH}_2\text{sal})_2]$. In contrast, the 3,3'-dianiline-derived ligand, ³CH₂salH₂, gives another type of dinuclear complex, $[\text{Zn}_2(^3\text{CH}_2\text{sal})_2]$, with a mosocate structure rather than a helicate structure. On the other hand, the 2,2'-dianiline-derived ligand, ²SsalH₂, produces a phenoxo-bridged dinuclear complex, $[\text{Zn}_2(^2\text{Ssal})_2]$. Such structural differences between the formed complexes occur depending on the relative positions of the two amino groups of the precursor dianiline. These distinguishable structural characteristics between the

Table 9

Selected vertical singlet excitations with the lowest energy or higher intensities ($f > 0.05$) for $[\text{Zn}_2(^2\text{Ssal})_2]$ from TD-DFT calculations at the S_0 geometry.

State	λ [nm]	Calculated		Observed ^a			
		Oscillator strength (f)	Main contributor	λ [nm]	Relative intensity ^b		
S ₁	409.25	0.0002	HOMO→LUMO (67.5%)	433.0	1.00		
S ₆	382.39	0.1427	HOMO-1→LUMO+2 (48.7%) HOMO→LUMO+3 (46.4%)				
S ₉	363.86	0.1765	HOMO-2→LUMO (83.1%)				
S ₁₀	360.21	0.1335	HOMO-3→LUMO (62.8%) HOMO-2→LUMO+1 (33.3%)				
S ₁₇	320.47	0.0798	HOMO-4→LUMO (90.9%)				
S ₂₇	298.37	0.0710	HOMO-7→LUMO (53.8%)				
S ₂₈	297.28	0.0879	HOMO-7→LUMO+1 (30.1%) HOMO-6→LUMO (58.3%)				
S ₄₀	287.48	0.0691	HOMO-7→LUMO+3 (35.6%) HOMO-6→LUMO+2 (29.0%)				
S ₄₁	284.05	0.0788	HOMO-2→LUMO+4 (47.6%)				
S ₄₂	283.78	0.0546	HOMO-3→LUMO+4 (36.3%) HOMO-2→LUMO+5 (47.0%)				
S ₅₁	276.7	0.0694	HOMO-11→LUMO (29.5%) HOMO-3→LUMO+5 (18.1%)	316.5	0.90		
S ₅₄	273.53	0.0669	HOMO-11→LUMO+1 (10.5%) HOMO-11→LUMO+2 (21.6%) HOMO-10→LUMO+3 (17.3%) HOMO-8→LUMO+2 (20.6%) HOMO-1→LUMO+9 (12.1%) HOMO→LUMO+8 (17.9%)				
S ₅₆	273.15	0.1363	HOMO-1→LUMO+9 (31.7%) HOMO→LUMO+8 (43.7%)				
S ₅₈	272.38	0.2258	HOMO-12→LUMO+1 (23.9%) HOMO-10→LUMO+1 (22.8%) HOMO-9→LUMO+1 (22.5%)				
S ₇₁	261.79	0.0565	HOMO-4→LUMO+4 (62.3%)				
S ₉₉	243.74	0.0836	HOMO-7→LUMO+5 (31.0%) HOMO-6→LUMO+4 (27.9%)				
S ₁₄₁	227.11	0.0717	HOMO-2→LUMO+12 (49.1%)			238.0	0.52
S ₁₄₇	224.74	0.0569	HOMO-8→LUMO+7 (19.4%) HOMO-6→LUMO+7 (35.5%)				

^a In the crystalline state.

^b Respect to the 433.0 nm band.

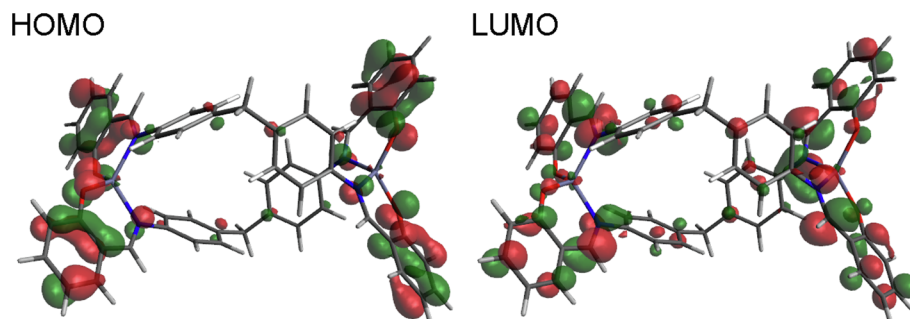


Fig. 5. Selected molecular orbital isosurfaces (0.03 ebohr^{-3}) for $[\text{Zn}_2(^4\text{CH}_2\text{sal})_2]$.

complexes reflect their luminescence properties. The Stokes shift of each complex is larger than that of the corresponding free ligand. Such larger Stokes shifts of the complexes are advantageous when considering the application as light emitting materials. Furthermore, the

emission maxima in the complexes are significantly shifted toward the higher-energy side compared to the ligands, indicating that the Zn(II) complexes produce luminescent colors that cannot be found in organic compounds alone. On the other hand, the Zn(II) complexes have

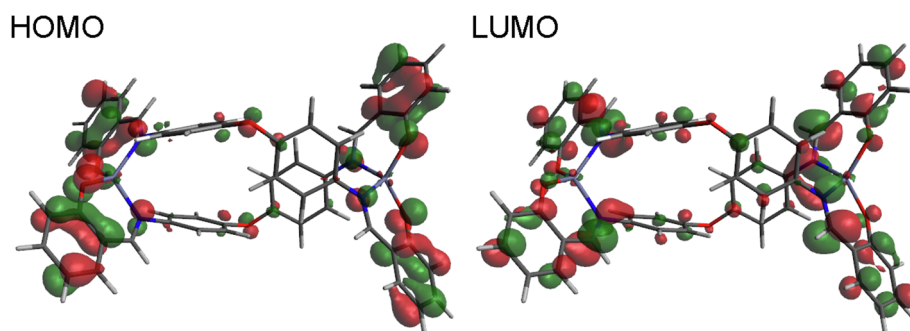


Fig. 6. Selected molecular orbital isosurfaces (0.03 ebohr^{-3}) for $[\text{Zn}_2(\text{}^4\text{Osal})_2]$.

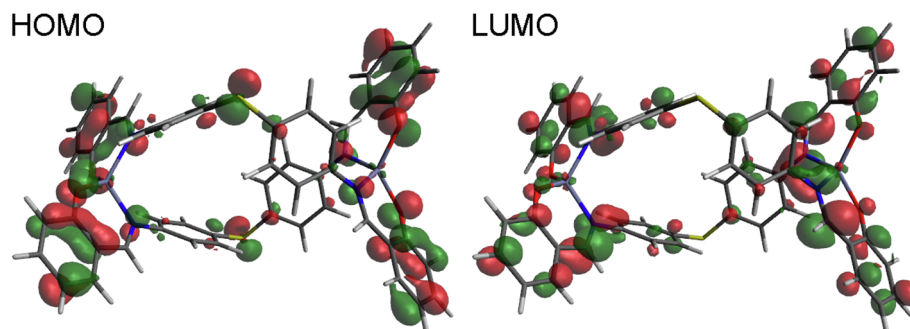


Fig. 7. Selected molecular orbital isosurfaces (0.03 ebohr^{-3}) for $[\text{Zn}_2(\text{}^4\text{Ssal})_2]$.

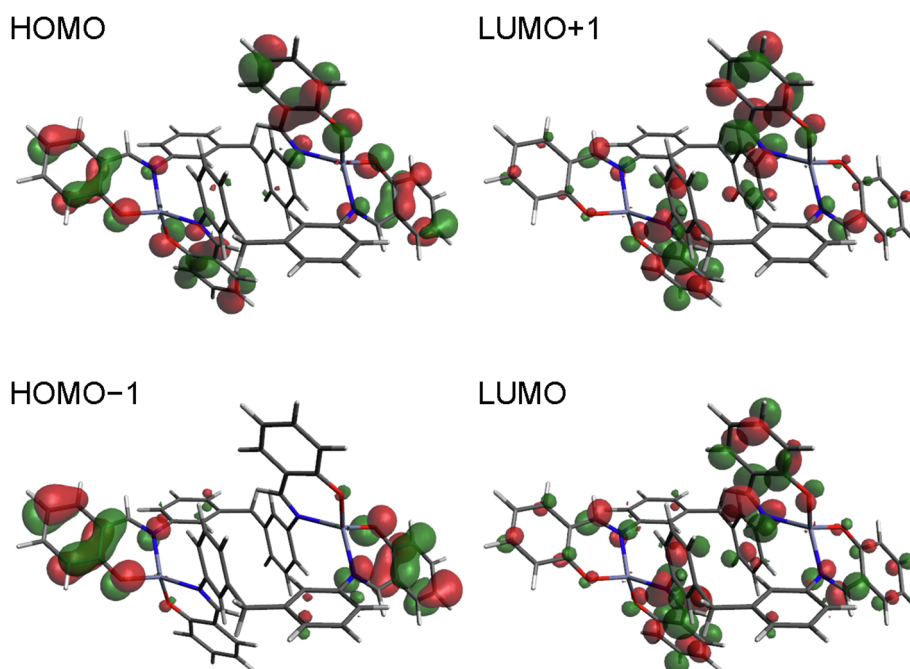


Fig. 8. Selected molecular orbital isosurfaces (0.03 ebohr^{-3}) for $[\text{Zn}_2(\text{}^3\text{CH}_2\text{sal})_2]$.

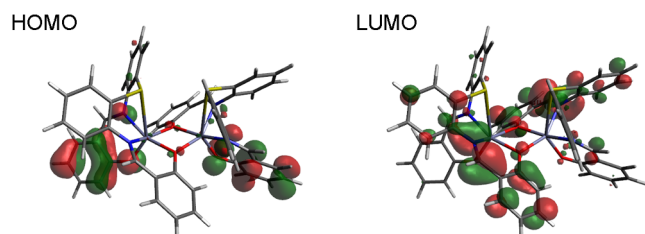


Fig. 9. Selected molecular orbital isosurfaces (0.03 ebohr^{-3}) for $[\text{Zn}_2(\text{}^2\text{Ssal})_2]$.

potential problems in their stabilities due to their d^{10} electron configurations. On synthesizing mononuclear complexes containing simple ligands, in particular, one may face difficulties in obtaining high yields. From this point of view as well, the present complexes have the merits of being obtained in high yields due to their rigidities and stabilities associated with polynuclearizations. It can be concluded therefore that the present dinuclear Zn(II) complexes have strong possibilities as luminescent materials.

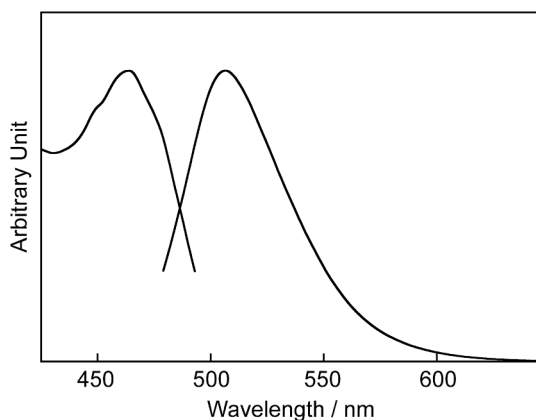


Fig. 10. Solid-state photoluminescence and excitation spectra of $[\text{Zn}_2(^4\text{OsSal})_2]$.

Table 10

The excitation (λ_{ex}) and emission wavelengths (λ_{em}), emission lifetimes (τ), and emission quantum yields (Φ_{em}) of $[\text{Zn}_2(^4\text{Msal})_2]$, $[\text{Zn}_2(^4\text{OsSal})_2]$, $[\text{Zn}_2(^4\text{Ssal})_2]$, $[\text{Zn}_2(^3\text{Msal})_2]$, and $[\text{Zn}_2(^2\text{Ssal})_2]$, together with those of the free ligands.

Complex	λ_{ex} [nm]	λ_{em} [nm]	Stokes shift [cm^{-1}]	τ [ns]	Φ_{em} [%]
$[\text{Zn}_2(^4\text{Msal})_2]$	462	501	1.68	1.97	12.0
$^4\text{MsalH}_2$	500	534	1.27	3.54	34.7
$[\text{Zn}_2(^4\text{OsSal})_2]$	464	506	1.79	2.56	17.4
$^4\text{OsSalH}_2$	489	532	1.65	0.59	2.7
$[\text{Zn}_2(^4\text{Ssal})_2]$	472	511	1.62	1.28	10.1
$^4\text{SsalH}_2$	497	534	1.39	1.67	13.1
$[\text{Zn}_2(^3\text{Msal})_2]$	464	506	1.79	1.57	5.4
$^3\text{MsalH}_2$	488	530	1.62	1.20	7.8
$[\text{Zn}_2(^2\text{Ssal})_2]$	481	520	1.56	1.42	7.5
$^2\text{SsalH}_2$	499	538	1.45	1.36	3.5

Acknowledgment

This work was supported by JSPS KAKENHI Grant Number JP19K05388.

Appendix A. Supplementary data

CCDC-1912177 for $[\text{Zn}_2(^4\text{OsSal})_2] \cdot 2\text{CH}_2\text{Cl}_2$, -1912178 for $[\text{Zn}_2(^4\text{Ssal})_2] \cdot 3\text{CH}_2\text{Cl}_2$, -1912179 for $[\text{Zn}_2(^3\text{CH}_2\text{sal})_2]$, and -1912180 for $[\text{Zn}_2(^2\text{Ssal})_2] \cdot 2\text{CH}_2\text{Cl}_2$ contain the supplementary crystallographic data for this paper. These data can be obtained free of charge at www.ccdc.cam.ac.uk/conts/retrieving.html [or from the Cambridge Crystallographic Data Center, 12, Union Road, Cambridge CB2 1EZ, UK; fax: +44 1223 336 033; E-mail: deposit@ccdc.cam.ac.uk]. Supplementary data to this article can be found online at <https://doi.org/10.1016/j.ica.2019.118979>.

References

- [1] F. Vögtle, E. Weber, *Angew. Chem. Int. Ed.* 18 (1979) 753.
- [2] J. Lehn, *Angew. Chem. Int. Ed.* 29 (1990) 1304.
- [3] A. Williams, *Chem. Eur. J.* 3 (1997) 15.
- [4] U. Knof, A. Von Zelewsky, *Angew. Chem. Int. Ed.* 38 (1999) 302.
- [5] M.D. Ward, J.A. McCleverty, J.C. Jeffery, *Coord. Chem. Rev.* 222 (2001) 251–272.
- [6] J.L. Atwood, L.J. Barbour, M.J. Hardie, C.L. Raston, *Coord. Chem. Rev.* 222 (2001) 3.
- [7] J.L. Serrano, T. Sierra, *Coord. Chem. Rev.* 242 (2003) 73.
- [8] J. Lewiński, J. Zachara, I. Justyniak, M. Dranka, *Coord. Chem. Rev.* 249 (2005) 1185.
- [9] M.H.V. Huynh, D.M. Dattelbaum, T.J. Meyer, *Coord. Chem. Rev.* 249 (2005) 457.
- [10] B.M. Zeglis, V.C. Pierre, J.K. Barton, *Chem. Commun.* (2007) 4565.

- [11] R. Ganguly, B. Sreenivasulu, J.J. Vittal, *Coord. Chem. Rev.* 252 (2008) 1027.
- [12] J. Stejskal, I. Sapurina, M. Trchova, *Prog. Polym. Sci.* 35 (2010) 1420.
- [13] H. Miyake, H. Tsukube, *Chem. Soc. Rev.* 41 (2012) 6977.
- [14] M. Boiocchi, L. Fabbri, *Chem. Soc. Rev.* 43 (2014) 1835.
- [15] O. Hietsoi, A.S. Filatov, C. Dubceac, M.A. Petrukhina, *Coord. Chem. Rev.* 295 (2015) 125.
- [16] A. Zask, G.A. Ellestad, *Chirality* 27 (2015) 589.
- [17] S. Miguez-Lago, M.M. Cid, *Synthesis* 49 (2017) 4111.
- [18] A.P. Paneerselvam, S.S. Mishra, D.K. Chand, *J. Chem. Sci.* 130 (2018) art. no. 96.
- [19] N. Yoshida, K. Ichikawa, *Chem. Commun.* (1997) 1091.
- [20] M.J. Hannon, C.L. Painting, A. Jackson, J. Hamblin, W. Errington, *Chem. Commun.* (1997) 1807.
- [21] N. Yoshida, H. Oshio, T. Ito, *Chem. Commun.* (1998) 63.
- [22] M.J. Hannon, C.L. Painting, N.W. Alcock, *Chem. Commun.* (1999) 2023.
- [23] N. Yoshida, H. Oshio, T. Ito, *J. Chem. Soc., Perkin Trans. 2* (1999) 975.
- [24] N. Yoshida, K. Ichikawa, M. Shiro, *J. Chem. Soc., Perkin Trans. 2* (2000) 17.
- [25] H. Cheng, D. Chun-ying, F. Chen-jie, M. Qing-jin, *J. Chem. Soc., Dalton Trans.* (2000) 2419.
- [26] P.E. Kruger, N. Martin, M. Nieuwenhuyzen, *J. Chem. Soc., Dalton Trans.* 1966 (2001).
- [27] L. Xua, X.-T. Chena, Y. Xua, D.-R. Zhua, X.-Z. Youa, L.-H. Weng, *J. Mol. Struct.* 559 (2001) 361.
- [28] P. Cai, M. Li, C.-Y. Duan, F. Lu, D. Guo, Q.-J. Meng, *New J. Chem.* 29 (2005) 1011.
- [29] G.I. Pascu, A.C.G. Hotze, C. Sanchez-Cano, B.M. Kariuki, M.J. Hannon, *Angew. Chem. Int. Ed.* 46 (2007) 4374.
- [30] U. McDonnell, M.R. Hicks, M.J. Hannon, A. Rodger, *J. Inorg. Biochem.* 102 (2008) 2052.
- [31] S.A. AbouEl-Enein, *J. Therm. Anal. Calorim.* 91 (2008) 929.
- [32] S. Dehghanpour, M. Khalaj, A. Mahmoudi, *Inorg. Chem. Commun.* 12 (2009) 231.
- [33] D.R. Boer, J.M.C.A. Kerckhoffs, Y. Parajo, M. Pascu, I. Usón, P. Lincoln, M.J. Hannon, M. Coll, *Angew. Chem. Int. Ed.* 49 (2010) 2336.
- [34] S. Dehghanpour, J. Lipkowski, A. Mahmoudi, M. Khalaj, *Polyhedron* 29 (2010) 2802.
- [35] C.A. Bear, J.M. Waters, T.N. Waters, *J. Chem. Soc. Sect. A* 2494 (1970).
- [36] R. Hernández-Molina, A. Mederos, P. Gili, S. Domínguez, F. Lloret, J. Cano, M. Julve, C. Ruiz-Pérez, X. Solans, *J. Chem. Soc. Dalton Trans.* 4327 (1997).
- [37] H. Torayama, T. Nishide, H. Asada, M. Fujiwara, T. Matsushita, *Polyhedron* 163787 (1997).
- [38] N. Kumari, R. Prajapati, L. Mishra, *Polyhedron* 27 (2007) 241.
- [39] M. Kondo, Y. Shibuya, K. Nabari, M. Miyazawa, S. Yasue, K. Maeda, F. Uchida, *Inorg. Chem. Commun.* 10 (2007) 1311.
- [40] Y. Yamada, T. Imari, D. Koori, *J. Coord. Chem.* 68 (2015) 1433.
- [41] L.J. Childs, N.W. Alcock, M.J. Hannon, *Angew. Chem. Int. Ed.* 40 (2001) 1079.
- [42] G.M. Sheldrick, *Acta Cryst. A* 64 (2008) 112.
- [43] M.C. Burla, R. Caliendo, M. Camalli, B. Carrozzini, G.L. Casciaro, L. De Caro, C. Giacovazzo, G. Polidori, D. Siliqi, R. Spagna, *J. Appl. Cryst.* 40 (2007) 609.
- [44] A.L. Spek, *Acta Cryst. C* 71 (2015) 9.
- [45] CrystalStructure 4.3: Crystal Structure Analysis Package, Rigaku Corporation, Tokyo 196-8666, Japan (2000–2018).
- [46] Gaussian 16, Revision B.01, M. J. Frisch, G. W. Trucks, H. B. Schlegel, G. E. Scuseria, M. A. Robb, J. R. Cheeseman, G. Scalmani, V. Barone, G. A. Petersson, H. Nakatsuji, X. Li, M. Caricato, A. V. Marenich, J. Bloino, B. G. Janesko, R. Gomperts, B. Mennucci, H. P. Hratchian, J. V. Ortiz, A. F. Izmaylov, J. L. Sonnenberg, D. Williams-Young, F. Ding, F. Lipparini, F. Egidi, J. Goings, B. Peng, A. Petrone, T. Henderson, D. Ranasinghe, V. G. Zakrzewski, J. Gao, N. Rega, G. Zheng, W. Liang, M. Hada, M. Ehara, K. Toyota, R. Fukuda, J. Hasegawa, M. Ishida, T. Nakajima, Y. Honda, O. Kitao, H. Nakai, T. Vreven, K. Throssell, J. A. Montgomery, Jr., J. E. Peralta, F. Ogliaro, M. J. Bearpark, J. J. Heyd, E. N. Brothers, K. N. Kudin, V. N. Staroverov, T. A. Keith, R. Kobayashi, J. Normand, K. Raghavachari, A. P. Rendell, J. C. Burant, S. S. Iyengar, J. Tomasi, M. Cossi, J. M. Millam, M. Klene, C. Adamo, R. Cammi, J. W. Ochterski, R. L. Martin, K. Morokuma, O. Farkas, J. B. Foresman, D. J. Fox, Gaussian, Inc., Wallingford CT, 2016.
- [47] A.D. Becke, *J. Chem. Phys.* 98 (1993) 5648.
- [48] C.T. Lee, W.T. Yang, R.G. Parr, *Phys. Rev. B* 37 (1988) 785.
- [49] P.C. Hariharan, J.A. Pople, *Theor. Chim. Acta* 28 (1973) 213.
- [50] M.M. Francl, W.J. Pietro, W.J. Hehre, J.S. Binkley, M.S. Gordon, D.J. Defrees, J.A. Pople, *J. Chem. Phys.* 77 (1982) 3654.
- [51] P.J. Hay, W.R. Wadt, *J. Chem. Phys.* 82 (1985) 299.
- [52] T. Keith, J. Millam, Gauss View, Version 5, R. Dennington, Semicem Inc., Shawnee Mission, 2009.
- [53] M.D. Hanwell, D.E. Curtis, D.C. Lonie, T. Vandermeersch, E. Zurek, G.R. Hutchison, *Avogadro: An advanced semantic chemical editor, visualization, and analysis platform*, *J. Cheminform.* 4 (2012) 17.
- [54] Experimental data for $[\text{Zn}_2(^4\text{CH}_2\text{sal})_2]$. Characteristic IR data [cm^{-1}]: 1256^m, 1610^s. Diffuse reflectance spectrum [λ_{max} , nm] (relative intensity respect to the 418.0 nm band): 418.0 (1.00), 319.5 (0.91), 238.0 (0.48).
- [55] Experimental data for $^4\text{CH}_2\text{salH}_2$. Characteristic IR data [cm^{-1}]: 1280^s, 1614^s, 2700^{br}. Diffuse reflectance spectrum [λ_{max} , nm] (relative intensity respect to the 418.0 nm band): 418.0 (1.00), 319.5 (0.91), 238.0 (0.48).
- [56] C. Demetgül, M. Karakaplan, S. Serin, M. Diğrak, *J. Coord. Chem.* 62 (2009) 3544.
- [57] M. Tümer, D. Ekinci, F. Tümer, A. Bulut, *Spectrochim. Acta Part A* 67 (2007) 916.